

Geophysical Research Letters®

RESEARCH LETTER

10.1029/2024GL109630

Potential Bias in Volcanic Paleomagnetic Records Due To Superimposed Chemical Remanent Magnetization



Key Points:

- We overprint a thermoremanent magnetization (TRM) by cooling from 600°C with a chemical remanent magnetization by 200 hr exposure at 400°C
- Chemical remanent magnetization was produced by the creation of cation-deficient titanomagnetite phases, then stabilized by oxyexsolution
- Paleodirections and intensities are strongly biased in the worst scenario, making the interpretation of characteristic components invalid

Supporting Information:

Supporting Information may be found in the online version of this article.

Correspondence to:

F. Lhuillier,
florian.lhuillier@lmu.de

Citation:

Shcherbakov, V. P., Lhuillier, F., Gribov, S. K., Tseltovich, V. A., & Aphinogenova, N. A. (2024). Potential bias in volcanic paleomagnetic records due to superimposed chemical remanent magnetization. *Geophysical Research Letters*, 51, e2024GL109630. <https://doi.org/10.1029/2024GL109630>

Received 4 APR 2024

Accepted 3 JUN 2024

V. P. Shcherbakov¹ , F. Lhuillier² , S. K. Gribov¹ , V. A. Tseltovich¹ , and N. A. Aphinogenova¹

¹Geophysical Observatory Borok, Yaroslavl'skaya Oblast, Russia, ²Department of Earth and Environmental Sciences, Ludwig-Maximilians-Universität, Munich, Germany

Abstract Volcanic rocks, preserving paleorecords of Earth's magnetic field, are essential to constrain the working of the geodynamo, provided their primary signal was not biased. Using a thermomagnetometer, we simulate a situation where a sample's primary record, carried by a thermoremanence (TRM, acquired by cooling in air from 600°C to room temperature), is partly overprinted by a chemical remanence (CRM, acquired by 200 hr of isothermal exposure at 400°C). This situation leads to two directional and intensity components (in the form of linear segments) in the Zijderveld and Arai-Nagata diagrams. In the case of unstable titanomagnetite grains prior to CRM acquisition, we show that both components can be strongly biased by up to ~50° for paleodirections and ~50% for paleointensities. In such a worst-case scenario, the secondary CRM strongly overprints the primary TRM, rendering the common interpretation of Zijderveld and Arai-Nagata diagrams in terms of characteristic components invalid.

Plain Language Summary Volcanic rocks, the magnetic minerals of which can acquire a thermoremanent magnetization (TRM) from Earth's magnetic field during their initial cooling, are essential to constrain the working of the geodynamo through Earth's history. However, if the rock is subsequently reheated at moderate temperature in another ambient field, the initial record can be partly overprinted by a chemical remanence (CRM). Starting from a TRM applied on materials of various thermostability, we reproduced in laboratory conditions the acquisition of a CRM by annealing the rock in a controlled ambient field for 200 hr at 400°C. Rock-magnetic and structural analyses at regular intervals, supplemented by continuous measurements of the remanent magnetization, indicate the creation of new phases as a result of oxidation processes. The paleomagnetic analysis of the final products reveals the existence of two distinct components that can be associated with the initial TRM and the secondary CRM. Whereas the paleomagnetic record of the initial TRM is trustworthy for the most stabilized initial products, directional (up to 50°) and intensity (up to 50%) biases are observed for the least stabilized initial products, illustrating a critical example where the interpretation of characteristic components (linear segments in the interpretation diagrams) is invalid.

1. Introduction

Volcanic rocks are widely used to constrain the variability (paleosecular variation; e.g., Dubrovine et al., 2019) and strength (virtual dipole moment; e.g., Bono et al., 2022) of Earth's magnetic field over the geological past. They usually bear a thermoremanent magnetization (TRM) acquired during the cooling of the magnetic minerals of a lava in the ambient field B_{anc} from above their Curie temperature T_C . In the ideal case of single-domain (SD) remanence carriers, the TRM direction is parallel to B_{anc} and the TRM intensity is proportional to $B_{\text{anc}} = |B_{\text{anc}}|$ (Néel, 1949, 1955).

As a TRM record may have been overprinted after the rock's emplacement, stepwise demagnetization is routinely used in paleomagnetism. Paleodirectional components—defined as straight lines in the vector endpoint diagrams—are interpreted as distinct records of Earth's magnetic field, the highest coercivity component corresponding to the primary paleodirection (e.g., Dunlop, 1979; Kirschvink, 1980; Zijderveld, 1967). Similarly, Thellier-style absolute paleointensity (API) experiments are conducted to simultaneously monitor the decay of the natural remanent magnetization (NRM) and the acquisition of a partial TRM (pTRM) in a laboratory field B_{lab} (Coe, 1967; Thellier & Thellier, 1959). Paleointensity components—defined as straight lines in the Arai-Nagata diagram (Nagata et al., 1963)—can be isolated following Thellier laws of reciprocity, independence and additivity (e.g., Dunlop, 2011).

© 2024. The Author(s).

This is an open access article under the terms of the [Creative Commons Attribution-NonCommercial-NoDerivs License](https://creativecommons.org/licenses/by/4.0/), which permits use and distribution in any medium, provided the original work is properly cited, the use is non-commercial and no modifications or adaptations are made.

Nevertheless, several complications may occur when analyzing the paleomagnetic record from volcanic rocks. On the one hand, an increase in magnetic grain size occasions a transition from SD to multidomain (MD) remanence carriers, with the twofold consequence that (a) palaeodirections are more easily overprinted due the lower coercivity of MD grains; and (b) Thellier laws are violated, leading to convex-shaped Arai-Nagata diagrams (e.g., Kosterov & Prévot, 1998; Nagy et al., 2022; Shcherbakov & Shcherbakova, 2001; Xu & Dunlop, 2004). On the other hand, chemical or structural changes occurring below T_C can be responsible for chemically induced remanences. Following Draeger et al. (2006)'s distinction, a remanence formed below T_C during a lava's initial cooling is termed thermochemical remanence (TCRM); a remanence arising from a prolonged exposure of an already solidified lava at a constant temperature $T < T_C$ is termed chemical remanence (CRM).

The suitability of (T)CRMs for API determinations has long been debated (e.g., Baker & Muxworthy, 2023; Draeger et al., 2006; Fabian, 2009; Lhuillier et al., 2023; Smirnov & Tarduno, 2005). We recently proposed that TCRMs produced by T_C increase may provide trustworthy API determinations whereas TCRMs produced by grain-size increase lead to erroneous API estimates (Shcherbakov et al., 2019, 2021). In this letter, we investigate the more complicated situation where a primary TRM is overprinted by a CRM, and the consequences thereof on the reliability of the directional and intensity records of the primary TRM.

2. Materials and Methods

All experiments from this study were conducted at the Borok Geophysical Observatory (BGO) of the Institute of Physics of the Earth of the Russian Academy of Sciences (IPE-RAS).

2.1. Volcanic Samples

Tholeiitic basalt from the axial part of the Reykjanes Ridge, collected during the fourth voyage (1982) of the research vessel “Akademik Mstislav Keldysh,” was chosen for the experiments. NRM is carried by titanomagnetite (TM) grains of small size ($\leq 4 \mu\text{m}$) and skeletal dendritic shape—typical for the rapid cooling of a lava under water—and TM has an ulvöspinel content of $\sim 52.5 \text{ mol}\%$ (Gribov et al., 2019). The measured $T_C = 168^\circ\text{C}$ (slightly higher than the expected $T_C = 158^\circ\text{C}$) indicates a low degree of low-temperature (LT) oxidation of the primary TM (e.g., Nishitani & Kono, 1983).

2.2. Thermal Treatment and Remanence Acquisition

For the remanence acquisition, a two-component rotating thermomagnetometer designed by Burakov–Vinogradov (IPE-RAS, Russia) was employed, while temperature was varied at a rate of $60^\circ\text{C}/\text{min}$ in a controlled magnetic environment. This instrument allows a constant monitoring of the horizontal component of the magnetic moment (with a noise threshold of $3 \cdot 10^{-9} \text{ Am}^2$) throughout a prolonged thermal treatment of up to several weeks.

Our experimental protocol is summarized in Figure 1a. Step 1 involved the thermal demagnetization of the samples from room temperature T_R to 600°C in a zero-field environment. Step 2 involved maintaining the samples at 600°C in air for a duration of 0 min (scenario 1), 4 min (scenario 2), 20 min (scenario 3) or 80 min (scenario 4), to produce materials of various composition and thermostability before imparting the remanences. Step 3 involved cooling down the samples from 600°C to T_R while applying a field ($B_{\text{lab}} = 50 \mu\text{T}$) along the y -axis, to mimic the acquisition of a primary TRM. Step 4 involved the partial demagnetization of the samples from T_R to 400°C in a zero-field environment. Step 5 involved exposing the samples at 400°C for a duration of 200 hr while applying a field ($B_{\text{lab}} = 50 \mu\text{T}$) along the x -axis, to mimic the acquisition of a secondary CRM. Step 6 finally involved cooling down the samples from 400°C to T_R while applying a field ($B_{\text{lab}} = 50 \mu\text{T}$) along the x -axis, with the consequence of imparting a pTRM. For simplicity, the resultant magnetization of the end product (remaining TRM + CRM + pTRM) is referred to RM in the rest of the manuscript.

2.3. Rock-Magnetic Experiments and Microscopic Observations

To explore the domain structure of the magnetic grains, hysteresis loops were measured using a Variable Field Translation Balance (VFTB, Petersen Instruments, Germany) on sister specimens at various stages of the heating treatment. After removal of the paramagnetic component (calculated above 0.6 T), the ratio of remanent

a. experimental protocol

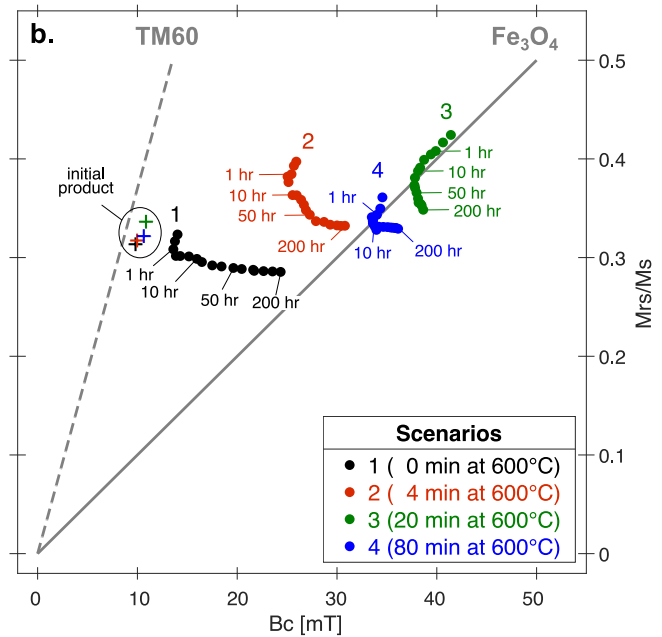
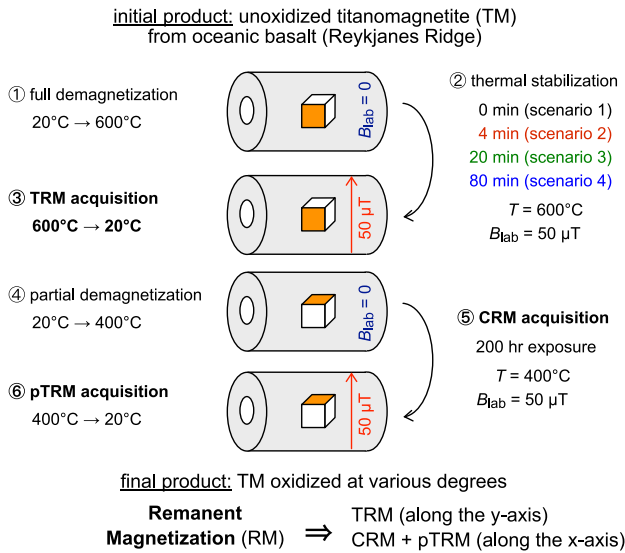


Figure 1. Thermal treatment applied to the samples. Panel (a): sketch of the protocol leading to the acquisition of a primary thermoremanent magnetization (TRM) along the y-axis (step 3), followed by the acquisition of a secondary chemical remanent magnetization (CRM) and partial TRM (pTRM) along the x-axis (steps 5–6). Four scenarios are considered to produce starting material of various composition and thermostability. Panel (b): time evolution of the hysteresis parameters in Néel (1955)'s diagram. The dashed and solid gray lines represent the reference curves for TM60 ($\text{Fe}_{2.4}\text{Ti}_{0.6}\text{O}_4$) and magnetite (Fe_3O_4 , Wang & Van der Voo, 2004).

saturation magnetization (M_{RS}) to saturation magnetization (M_S) was plotted against coercivity (B_C) in Néel (1955)'s diagram (e.g., Roberts et al., 2019; Tauxe et al., 2002).

To characterize the thermomagnetic behavior of the magnetic grains, continuous thermomagnetic curves $M_S(T)$ were measured in $B_{\text{lab}} = 0.45 \text{ T}$ using a ferromagnetic fraction analyzer (Orion, Russia). The Curie points of the ferrimagnetic phases were associated with the minima of the first derivative of the heating branches of the $M_S(T)$ curves (e.g., Fabian et al., 2013; Tauxe, 1998).

To confirm the nature of the magnetic grains, scanning electron microscopy (SEM) was performed using a VEGA II LMU device (TESCAN, Czech Republic) equipped with an energy dispersive X-ray analyzer INCA ENERGY 450 (Oxford Instruments, United-Kingdom). The magnetic fraction of the samples was analyzed using a multifunctional powder X-ray spectrometer STADI MP (STOE, Germany) and the diffraction peaks were compared with the reference values from the ICDD PDF-2 powder diffraction database (2004 version; Gates-Rector & Blanton, 2019).

2.4. Absolute Palaeointensity Experiments

Thellier-Coe experiments (Coe, 1967; Thellier & Thellier, 1959) including pTRM checks (Coe et al., 1978; Prévot et al., 1983) and pTRM tail checks (Riisager & Riisager, 2001) were conducted on the end products of the four heating scenarios described in Section 2.2, to monitor the temperature dependency of the ratio b of the remaining RM to the acquired laboratory pTRM while tracking the trajectory of the end point of the RM vector. For a given temperature range, the paleointensity estimate is $B = |b| \cdot B_{\text{lab}}$ ($B_{\text{lab}} = 50 \mu\text{T}$ in our case), where b corresponds to the slope estimate of the best-fit line in the Arai-Nagata diagram. To quantify chemical alteration during the experiments, we used the DRAT parameter, defined as the maximum absolute difference produced by a pTRM check, normalized by the length of best-fit line (Selkin & Tauxe, 2000).

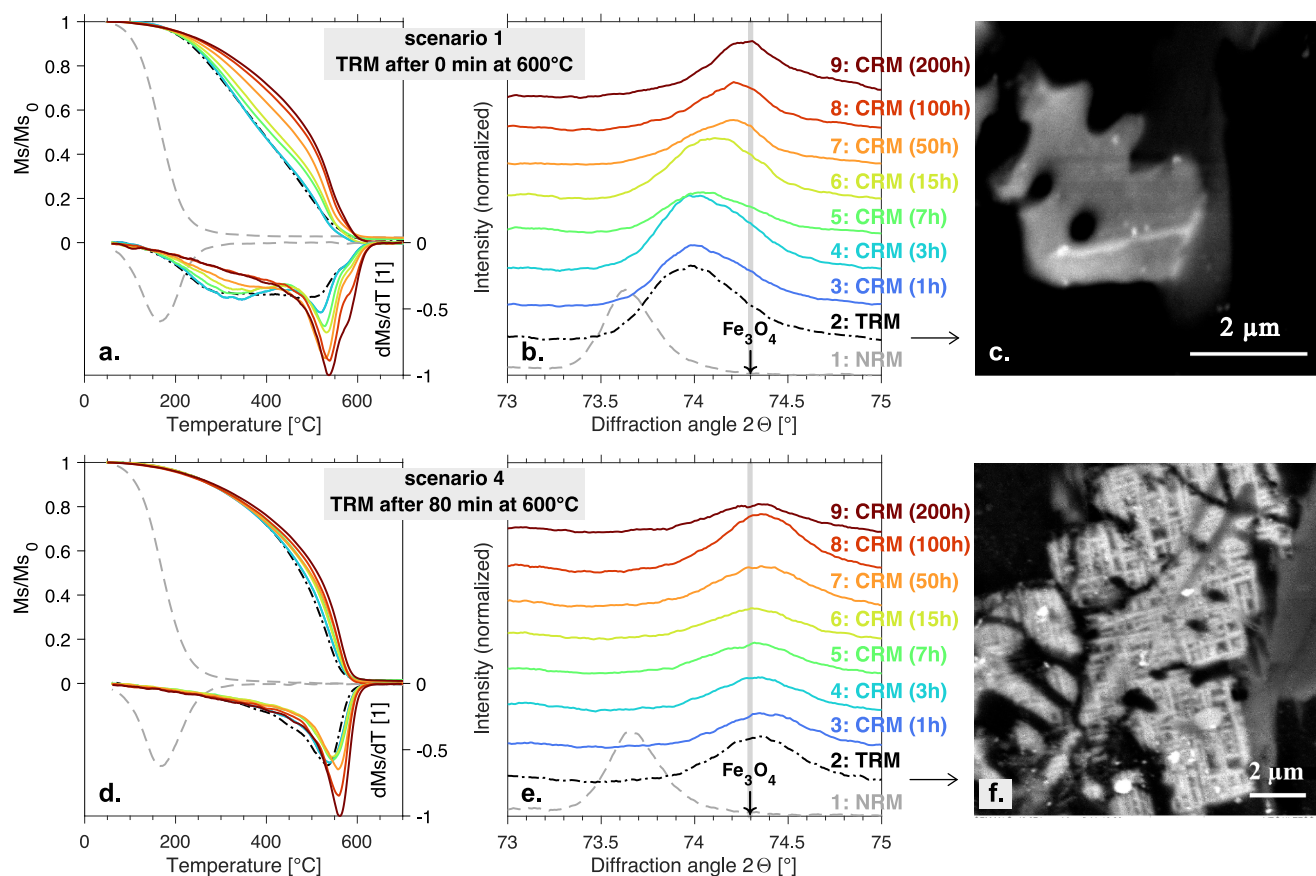


Figure 2. Monitoring of the magneto-mineralogical changes throughout the thermal treatment for scenario 1 (Panels a–c; thermoremanent magnetization (TRM) acquired after 0 min at 600°C) and scenario 2 (Panels d–f; TRM acquired after 80 min at 600°C). Panels (a) and (d): normalized thermomagnetic curves of saturation magnetization M_S (left axis) and their first derivative (right axis). Panels (b) and (e): normalized diffractograms in the region of the (440) reflection of the spinel phase. Panels (c) and (f): microphotographs of polished sections conducted between step 2 and step 3 of the thermal treatment.

3. Results

3.1. Magneto-Mineralogical Changes

In terms of hysteresis parameters, the initial samples prior to isothermal exposure at 600°C lie in the vicinity the reference curve for $\text{Fe}_{2.4}\text{Ti}_{0.6}\text{O}_4$ (TM60) in the Néel diagram (Figure 1b and Figure S1 in Supporting Information S1; Wang & Van der Voo, 2004). At the onset of the isothermal exposure to 400°C, the sample for scenario 1 is located to the right of the TM60 reference curve, whereas samples for scenarios 3 and 4 are close to the reference curve for magnetite (Wang & Van der Voo, 2004), indicating that TM grains from these latter scenarios were already partly oxyexsolved at the end of the exposure at 600°C. During the first hours of the exposure at 400°C (~1 hr for scenarios 1–2; ~10 hr for scenarios 3–4), M_{RS}/M_S and B_C simultaneously decrease (i.e., the points follow a southwest trajectory, parallel to the references curves, in the Néel diagram), suggesting that TM does not change its titanium content but likely experiences LT oxidation. In a second stage, M_{RS}/M_S continues decreasing (i.e., M_S continues increasing as M_{RS} is nearly constant in our experiments) but B_C increases, suggesting the ongoing oxyexsolution of the TM grains.

In terms of thermomagnetic behavior, the $M_S(T)$ curves of the initial samples prior to isothermal exposure at 600°C are characterized by a well-defined T_C around 168°C (Figure 2a for scenario 1; Figure 2d for scenario 4). The most clearly expressed changes in the $M_S(T)$ curves occur after the initial heating to 600°C. On the one hand, a flat minimum in the derivative of the $M_S(T)$ curve is observed at low temperature (200–400°C), pointing to a wide spectrum of T_C in this temperature interval, due to inhomogeneous LT oxidation of the initial TM grains. This feature tends to vanish after ~50 hr of isothermal exposure at 400°C, suggesting an advanced stage of LT oxidation with the formation of metastable cation-deficient TM. On the other hand, a sharp minimum of dM_S/dT is

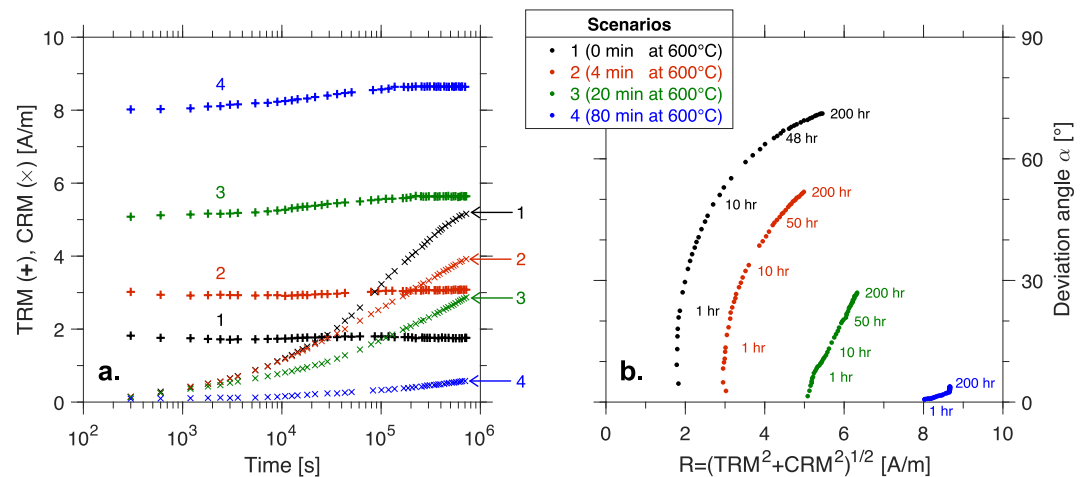


Figure 3. Monitoring of the remanence in the course of the chemical remanent magnetization (CRM) acquisition for the four considered scenarios. Panel (a): remaining thermoremanent magnetization (TRM, plus symbols) and acquired CRM (cross symbols) as a function of the duration of isothermal exposure at 400°C. Panel (b): deviation angle of the total remanent magnetization with respect to the y-axis (direction of the original TRM) as a function of the norm of the total remanent magnetization.

observed in the 510–530°C range, the relative amplitude of which increases with the duration of the isothermal exposure at 400°C. The center of this peak moves from 510–530°C to 540–560°C, suggesting the oxyexsolution of the TM grains leading to an end product close to magnetite. More generally, the longer the initial heating to 600°C, the faster the degeneration of the low-temperature phase (Figure S2 in Supporting Information S1). This can be explained by the fact that oxyexsolution having occurred at 600°C stabilizes the TM grains, which become in turn less prone to LT oxidation.

In terms of structural analysis, the initial heating to 600°C leads to a noticeable shift to the right of the (440) reflection and to a broadening of its profile (Figure 2b for scenario 1; Figure 2e for scenario 4). The longer the initial exposure to 600°C, the more pronounced the intensity of the shift (Figure S3 in Supporting Information S1). Subsequent exposure at 400°C leads to a progressive shift to the right of the (440) reflection. These changes indicate a decrease in the cell size of the cubic unit, to reach an end product close to magnetite. At the same time, the (104) reflection of the hexagonal phase reveals the increasing presence of small fractions of ilmenite (from 0.5% to 3%) and hematite (from 2% to 3%; Figure S4 in Supporting Information S1). These observations once more suggest the oxyexsolution of the TM grains with an ilmenite-magnetite intergrowth.

SEM observations confirm that the oxyexsolution of TM grains starts immediately after the initial heating to 600°C. For scenario 1 (0 min pause at 600°C), Figure 2c shows heterogeneous areas with isolated ilmenite precipitates in the form of thin lamellae (up to 30 nm width). For scenario 4 (80 min exposure at 600°C), Figure 2f shows the presence of a magnetite-ilmenite intergrowth (treillis-like texture with lamellae of 120–150 nm width) occupying the entire volume of the TM grains. Observations for scenarios 2 and 3 reveal intermediate degrees of oxyexsolution, with numerous parallel lamellae (of 50–70 nm width) appearing within the TM matrix for scenario 2 (4 min of exposure at 600°C, Figure S5 in Supporting Information S1) and the transition from a sandwich-type to a treillis-type texture with lamellae (of 70–100 nm width) for scenario 3.

3.2. Time Monitoring of the Remanence Acquisition

Figure 3 describes the monitoring of the remanence (TRM remaining along the y-axis; CRM acquired along the x-axis) during the 200 hr of isothermal exposure at 400°C. The shorter the duration of the sample's initial isothermal exposure at 600°C (i.e., the lower the degree of magneto-mineralogical transformations of the initial TM), the higher the final amplitude of the CRM (Figure 3a, cross symbols). In particular, the final amplitude of the CRM in the case of scenario 1 (0 min of initial exposure at 600°C, black symbols) and scenario 2 (4 min of initial exposure at 600°C, red symbols) exceeds the initial value of the TRM. During the prolonged exposure at 400°C, the TRM amplitude remains nearly constant for scenarios 1–2 (Figure 3a, plus symbols), whereas it increases by ~11% for scenario 3 (20 min of initial exposure at 600°C, green symbols) and by ~8% for scenario 4 (80 min of initial

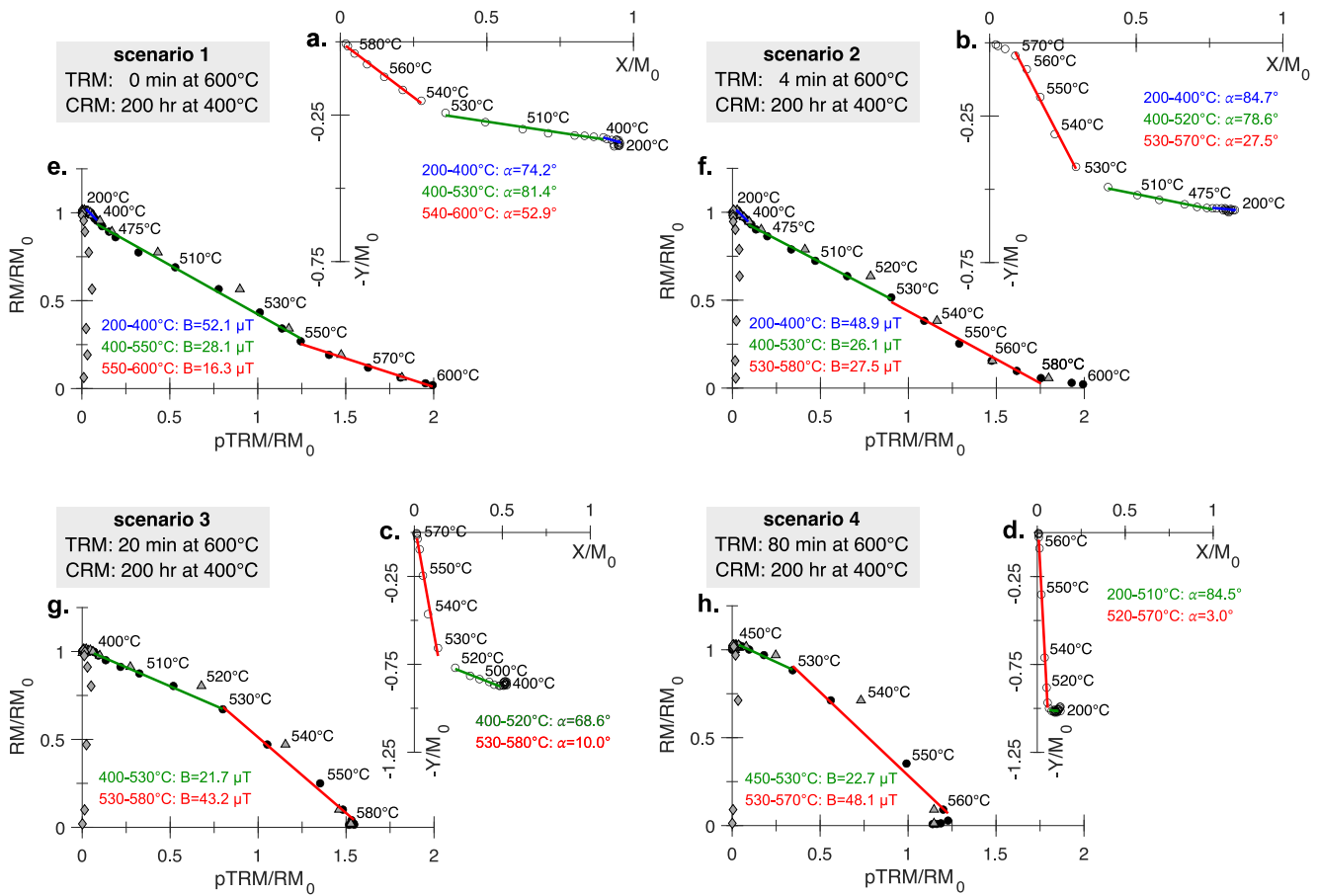


Figure 4. Paleomagnetic analysis of the final samples for the four considered scenarios. Panels (a–d): Zijderveld diagrams used to analyze the directional record from the remanent magnetization RM. The quantity α is the deviation angle from the x -axis. Panels (e–h): Arai-Nagata diagrams used to analyze the intensity record from RM. Triangle symbols stand for pTRM checks, diamond symbols represent pTRM tail checks. The quantity B is the paleointensity estimate.

exposure at 600°C, blue symbols). The reinforcement of the TRM amplitude is likely ascribable to an increase in T_C due to continuation of the oxyexsolution process of TM grains.

Figure 3b shows the trajectory of the remanence amplitude R and of the deviation angle α of the end point of the remanence vector with respect to the y -axis (i.e., the direction in which the TRM was applied) in the course of the CRM acquisition. As expected, the vector rotates from the direction of the initial TRM toward the direction in which the CRM was applied, while R increases. The shorter the duration of the sample's initial isothermal exposure at 600°C, the stronger the value of α (reaching 71° for scenario 1) and the lower the final value of R .

3.3. Directional Analysis of the Remanence

Figures 4a–4d show the evolution of the end point of the RM vector in the course of the Thellier-Coe protocol. In four scenarios, a high-temperature (HT) segment is identified from 520–540°C to 570–600°C (red curves; Figures 4a–4d), the length of which increases from scenario 1 to 4. In four scenarios, a distinct mid-temperature (MT) segment is identified from ~400°C to 510–530°C (green curves; Figures 4a–4d), the length of which decreases from scenario 1 to 4. Finally, in scenarios 1 and 2 only, a low-temperature (LT) segment is identified from ~200°C to ~400°C (blue curves; Figures 4a and 4b), the length of which is negligible compared to the MT and HT segments. The LT and MT segments depart by 5–20° from the x -axis (i.e., the direction in which the CRM was applied), with no obvious trend from scenario 1 to 4. The HT segment departs from the y -axis (i.e., the direction in which the TRM was applied) by an angle decreasing from 53° (scenario 1) to 3° (scenario 4).

3.4. Absolute Paleointensity Analysis of the Remanence

Consistent with the directional analysis (Figures 4a–4d), two to three linear segments are identified in the Arai-Nagata diagrams (Figures 4e–4h; Table S1 in Supporting Information S1), with the same inflection points at $\sim 400^\circ\text{C}$ and $530\text{--}550^\circ\text{C}$. The LT segment yields $B = 52\ \mu\text{T}$ for scenario 1 (Figure 4e) and $B = 49\ \mu\text{T}$ for scenario 2 (Figure 4f), closely coinciding with the field applied during the remanence acquisition ($B_{\text{lab}} = 50\ \mu\text{T}$). The MT segment yields B values decreasing from 26 to 28 μT for scenarios 1–2 (Figures 4e and 4f) to 22–23 μT for scenarios 3–4 (Figures 4g and 4h), that is, values 45%–55% lower than $B_{\text{lab}} = 50\ \mu\text{T}$. The HT segment yields B values increasing from 16 μT for scenario 1 (Figure 4e) to 48 μT for scenario 4 (Figure 4h). For scenario 2, note the specificity that the MT and HT segments yield nearly indistinguishable values (Figure 4f), in contrast with the directional analysis (Figure 4b). Whereas DRAT does not exceed 10% for the LT and MT segments, its value is on the order of 14%–16% for the HT segment (Table S1 in Supporting Information S1), pointing to the occurrence of enhanced chemical changes in this HT range. pTRM tail checks conducted for the samples of scenarios 1, 2 and 4 (Figures 4e, 4f and 4h) are positive and confirm that the remanence is borne by SD-like carriers.

4. Discussion

The raison d'être of our experiments was to simulate a situation where the primary remanence of a tholeiitic basalt, carried by a TRM (acquired by cooling in $B_{\text{lab}} = 50\ \mu\text{T}$ from 600°C to T_R), was overprinted by a CRM (acquired by prolonged isothermal exposure at 400°C in $B_{\text{lab}} = 50\ \mu\text{T}$). The thermostability of the starting material was controlled by the duration of the isothermal exposure at 600°C (from 0 min in scenario 1 to 80 min in scenario 4), to produce TM phases with decreasing metastable cation-deficient TM content. To facilitate the monitoring of the remanence, the TRM and CRM were imparted in orthogonal directions. Magneto-mineralogical observations revealed that the CRM was formed due to the emergence of new ferrimagnetic phases with $T_C > 400^\circ\text{C}$ (Figure 2). These phases were first produced by the LT oxidation of the unstable TM fraction, and second by the oxyexsolution of the newly formed cation-deficient phases. The amplitude of the CRM greatly depended on the duration of the initial exposure, with CRM/TRM₀ decreasing from ~ 2.8 in scenario 1 to ~ 0.06 in scenario 4 (Figure 3a). Conversely, the TRM intensity remained nearly constant during the CRM acquisition, indicating that (a) the CRM carriers were new physical phases, and (b) the TRM carriers were little impacted by the exposure to 400°C . This implies that the TRM carriers were mainly stabilized oxyexsolved volumes of TM grains, generated immediately after the initial exposure to 600°C . Indeed, in the case of scenario 2, thin ilmenite plates in the space between the primary formed ilmenite lamellae were detected after exposure at 400°C , compatible with the oxyexsolution of newly formed cation-deficient titanomagnetites and constituting a rare observation of secondary oxyexsolution (Figure S5f in Supporting Information S1).

The paleomagnetic analysis of the end products revealed two to three linear segments in the Zijdeveld and Arai-Nagata diagrams. The HT segment above $\sim 530^\circ\text{C}$ can be associated with the remaining TRM, contaminated by the HT fraction of the CRM produced by oxyexsolution of the metastable titanomaghemite. The MT segment between $\sim 400^\circ\text{C}$ and $\sim 530^\circ\text{C}$ can be associated with the fraction of the CRM produced by the LT oxidation of the unstable TM fraction, supplemented by the MT fraction of the remaining TRM. Finally, the LT component between $\sim 200^\circ\text{C}$ and $\sim 400^\circ\text{C}$ corresponds to the pTRM acquired during the last cooling from 400°C to TR T_R .

In terms of directions, the LT component, with a negligible remanence fraction of $\sim 5\%$, is only observed for scenarios 1 and 2 (i.e., for the most unstable starting products). Its direction departs by $5\text{--}15^\circ$ from the direction in which the pTRM was applied, likely as a result of uncertainty in sample orientation. The MT directional component is clearly visible for scenarios 1–3 but is largely suppressed for scenario 4. The best-fit direction for scenarios 1–3 departs by $10\text{--}20^\circ$ from the direction in which the CRM was applied, leading to moderately biased results if the secondary component was interpreted as a purely thermal overprint. Finally, the HT directional component yields for scenario 4 (i.e., for the most stable starting product) a reliable record of the direction in which the TRM was applied. With increasing the instability of the initial TM (from scenario 3 to 1), the deviation of the best-fit direction from the direction in which the TRM was applied gradually increases from $\sim 10^\circ$ (scenario 3) to $\sim 53^\circ$ (scenario 1). Such scenarios of overlapping coercivity spectra would be problematic in paleomagnetism since difficult to detect (e.g., Butler, 1992; Dunlop, 1979). On the one hand, the decay of the vector endpoints toward the origin is commonly interpreted as a proof of the primary nature of the remanence. On the other hand, microscopic observations would be inconclusive to determine whether the magneto-mineralogical

changes (evidenced by the relics of the oxidation processes in the TM grains) occurred after the rock's initial cooling.

In terms of intensities, the LT component, although giving the right intensity estimate, would be discarded due to the negligible remanence fraction of ~6%. The MT component, which may pass the modified PICRIT03 and SELCRIT02 selection criteria on the individual Arai-Nagata diagrams (e.g., Paterson et al., 2014), yields an intensity underestimated by 45%–55%. Knowing that the largest contribution of the MT segment stems from the CRM, such an underestimation is not surprising and consistent with previous experimental results (e.g., Baker & Muxworthy, 2023; Gribov et al., 2017; Gribov et al., 2019). Finally, the HT component only gives the right intensity estimate for scenario 4. When increasing the metastable cation-deficient TM content of the initial TM, the intensity is underestimated from ~15% in scenario 3–~65% in scenario 1.

More generally, two-sloped Arai-Nagata diagrams are often encountered in archeo- and paleomagnetism. When the remanence carriers are SD-like and the two components are simultaneously observed in the Zijdeveld and Arai-Nagata diagrams, it is often accepted that the highest and lowest temperature slope give reliable records of the paleofields when the primary and secondary remanence were respectively acquired (e.g., Lloyd et al., 2021; Monster et al., 2018; Shcherbakova et al., 2020; Thallner et al., 2022). We show in this paper that such an interpretation, expected to be valid in the case of a thermal overprint on stabilized initial TM, may be largely erroneous in the case when a CRM was produced on unstable initial TM. Contrary to the well-accepted conception that LT oxidation only impairs the intensity records of volcanic rocks or archeological artifacts, we also stress that CRM overprints on unstable initial TM, may render the interpretation of Zijdeveld diagrams in terms of characteristic components largely invalid.

Data Availability Statement

Required information to reproduce the experiments is provided in Section 2. Required data to reproduce the figures are available at Open Data LMU (Shcherbakov et al., 2024).

Acknowledgments

This study was supported by the State Program of GO Borok (SKG, VAT, NAA), and DFG Grant 517539177 (FL). The paleointensity experiments were supported by RSF Grant number 23-17-00112 (VPS). We thank Monika Korte for editorial handling; Lisa Tauxe and Karl Fabian for their constructive reviews that helped improve the manuscript. Open Access funding enabled and organized by Projekt DEAL.

References

- Baker, E. B., & Muxworthy, A. R. (2023). Using Preisach theory to evaluate chemical remanent magnetization and its behavior during Thellier-Thellier-Coe paleointensity experiments. *Journal of Geophysical Research: Solid Earth*, 128(2), e2022JB025858. <https://doi.org/10.1029/2022jb025858>
- Bono, R. K., Paterson, G. A., & Biggin, A. J. (2022). MCADAM: A continuous paleomagnetic dipole moment model for at least 3.7 billion years. *Geophysical Research Letters*, 49(21), e2022GL100898. <https://doi.org/10.1029/2022gl100898>
- Butler, R. F. (1992). *Paleomagnetism: Magnetic domains to geologic terranes*. Blackwell Science.
- Coe, R. S. (1967). The determination of paleo-intensities of the Earth's magnetic field with emphasis on mechanisms which could cause non-ideal behavior in Thellier's method. *Journal of Geomagnetism and Geoelectricity*, 19(3), 157–179. <https://doi.org/10.5636/jgg.19.157>
- Coe, R. S., Grommé, C. S., & Mankinen, E. A. (1978). Geomagnetic paleointensities from radiocarbon-dated lava flows on Hawaii and the question of the Pacific nondipole low. *Journal of Geophysical Research*, 83(B4), 1740–1756. <https://doi.org/10.1029/JB083iB04p01740>
- Dobrovine, P. V., Veikkolainen, T., Pesonen, L. J., Piispa, E., Ots, S., Smirnov, A. V., et al. (2019). Latitude dependence of geomagnetic paleosecular variation and its relation to the frequency of magnetic reversals: Observations from the Cretaceous and Jurassic. *Geochemistry, Geophysics, Geosystems*, 20(3), 1240–1279. <https://doi.org/10.1029/2018GC007863>
- Draeger, U., Prévot, M., Poidras, T., & Riisager, J. (2006). Single-domain chemical, thermochemical and thermal remanences in a basaltic rock. *Geophysical Journal International*, 166(1), 12–32. <https://doi.org/10.1111/j.1365-246X.2006.02862.x>
- Dunlop, D. J. (1979). On the use of Zijdeveld vector diagrams in multicomponent paleomagnetic studies. *Physics of the Earth and Planetary Interiors*, 20(1), 12–24. [https://doi.org/10.1016/0031-9201\(79\)90103-1](https://doi.org/10.1016/0031-9201(79)90103-1)
- Dunlop, D. J. (2011). Physical basis of the Thellier-Thellier and related paleointensity methods. *Earth and Planetary Science Letters*, 187(3–4), 118–138. <https://doi.org/10.1016/j.pepi.2011.03.006>
- Fabian, K. (2009). Thermochemical remanence acquisition in single-domain particle ensembles: A case for possible overestimation of the geomagnetic paleointensity. *Geochemistry, Geophysics, Geosystems*, 10(6). <https://doi.org/10.1029/2009GC002420>
- Fabian, K., Shcherbakov, V. P., & McEnroe, S. A. (2013). Measuring the Curie temperature. *Geochemistry, Geophysics, Geosystems*, 14(4), 947–961. <https://doi.org/10.1029/2012GC004440>
- Gates-Rector, S., & Blanton, T. (2019). The powder diffraction file: A quality materials characterization database. *Powder Diffraction*, 34(4), 352–360. <https://doi.org/10.1017/S0885715619000812>
- Gribov, S. K., Dolotov, A. V., & Shcherbakov, V. P. (2017). Experimental modeling of the chemical remanent magnetization and Thellier procedure on titanomagnetite-bearing basalts. *Izvestiya - Physics of the Solid Earth*, 53(2), 274–292. <https://doi.org/10.1134/s1069351317010062>
- Gribov, S. K., Shcherbakov, V. P., & Aphinogenova, N. A. (2019). Magnetic properties of artificial CRM created on titanomagnetite-bearing Oceanic basalts. In D. Nurgaliev, V. Shcherbakov, A. Kosterov, & S. Spassov (Eds.), *Recent advances in rock magnetism, environmental magnetism and paleomagnetism* (pp. 173–194). Springer International Publishing.
- Kirschvink, J. L. (1980). The least-squares line and plane and the analysis of palaeomagnetic data. *Geophysical Journal of the Royal Astronomical Society*, 62(3), 699–718. <https://doi.org/10.1111/j.1365-246X.1980.tb02601.x>

- Kosterov, A. A., & Prévot, M. (1998). Possible mechanisms causing failure of Thellier palaeointensity experiments in some basalts. *Geophysical Journal International*, 134(2), 554–572. <https://doi.org/10.1046/j.1365-246x.1998.00581.x>
- Lhuillier, F., Shcherbakov, V. P., & Sycheva, N. K. (2023). Detecting dipolarity of the geomagnetic field in the paleomagnetic record. *Proceedings of the National Academy of Sciences of the United States of America*, 120(25), e2220887120. <https://doi.org/10.1073/pnas.2220887120>
- Lloyd, S. J., Biggin, A. J., Halls, H., & Hill, M. J. (2021). First palaeointensity data from the cryogenian and their potential implications for inner core nucleation age. *Geophysical Journal International*, 226(1), 66–77. <https://doi.org/10.1093/gji/ggab090>
- Monster, M. W. L., van Galen, J., Kuiper, K. F., Dekkers, M. J., & de Groot, L. V. (2018). A late-quaternary full-vector geomagnetic record from El Golfo section, El Hierro, Canary Islands. *Geophysical Journal International*, 215(3), 1701–1717. <https://doi.org/10.1093/gji/ggy361>
- Nagata, T., Arai, Y., & Momose, K. (1963). Secular variation of the geomagnetic total force during the last 5000 years. *Journal of Geophysical Research*, 68(18), 5277–5281. <https://doi.org/10.1029/j.2156-2202.1963.tb00005.x>
- Nagy, L., Williams, W., Tauxe, L., & Muxworthy, A. (2022). Chasing tails: Insights from micromagnetic modeling for thermomagnetic recording in non-uniform magnetic structures. *Geophysical Research Letters*, 49(23), e2022GL101032. <https://doi.org/10.1029/2022gl101032>
- Néel, L. (1949). Théorie du trainage magnétique des ferromagnétiques en grains fins avec applications aux terres cuites. *Annales de Geophysique*, 5, 99–136.
- Néel, L. (1955). Some theoretical aspects of rock-magnetism. *Advances in Physics*, 4(14), 191–243. <https://doi.org/10.1080/00018735500101204>
- Nishitani, T., & Kono, M. (1983). Curie temperature and lattice constant of oxidized titanomagnetite. *Geophysical Journal of the Royal Astronomical Society*, 74, 585–600. <https://doi.org/10.1111/j.1365-246X.1983.tb01890.x>
- Paterson, G. A., Tauxe, L., Biggin, A. J., Shaar, R., & Jonestrask, L. C. (2014). On improving the selection of Thellier-type paleointensity data. *Geochemistry, Geophysics, Geosystems*, 15(4), 1180–1192. <https://doi.org/10.1002/2013GC005135>
- Prévot, M., Mankinen, E. A., Grommé, S., & Lecaille, A. (1983). High paleointensities of the geomagnetic field from thermomagnetic studies on Rift Valley pillow basalts from the Mid-Atlantic Ridge. *Journal of Geophysical Research*, 88(B3), 2316–2326. <https://doi.org/10.1029/JB088iB03p02316>
- Riisager, P., & Riisager, J. (2001). Detecting multidomain magnetic grains in Thellier palaeointensity experiments. *Physics of the Earth and Planetary Interiors*, 125(1–4), 111–117. [https://doi.org/10.1016/S0031-9201\(01\)00236-9](https://doi.org/10.1016/S0031-9201(01)00236-9)
- Roberts, A. P., Hu, P., Harrison, R. J., Heslop, D., Muxworthy, A. R., Oda, H., et al. (2019). Domain state diagnosis in rock magnetism: Evaluation of potential alternatives to the day diagram. *Journal of Geophysical Research: Solid Earth*, 124(6), 5286–5314. <https://doi.org/10.1029/2018jb017049>
- Selkin, P. A., & Tauxe, L. (2000). Long-term variations in palaeointensity. *Philosophical Transactions of the Royal Society of London, Series A*, 358(1768), 1065–1088. <https://doi.org/10.1098/rsta.2000.0574>
- Shcherbakov, V. P., Gribov, S. K., Lhuillier, F., Aphinogenova, N. A., & Tsel'movich, V. A. (2019). On the reliability of absolute palaeointensity determinations on basaltic rocks bearing a thermochemical remanence. *Journal of Geophysical Research: Solid Earth*, 117(3), 7616–7632. <https://doi.org/10.1029/2019JB017873>
- Shcherbakov, V. P., Lhuillier, F., Gribov, S. K., Tsel'movich, V. A., & Aphinogenova, N. A. (2024). Raw data from the publication "potential Bias in volcanic paleomagnetic records due to superimposed chemical remanent magnetization" [Dataset]. *Open Data LMU*. <https://doi.org/10.5282/ubm/data.490>
- Shcherbakov, V. P., Lhuillier, F., & Sycheva, N. K. (2021). Exact analytical solutions for kinetic equations describing thermochemical remanence acquisition for single-domain grains: Implications for absolute paleointensity determinations. *Journal of Geophysical Research: Solid Earth*, 126(5), e2020JB021536. <https://doi.org/10.1029/2020jb021536>
- Shcherbakov, V. P., & Shcherbakova, V. V. (2001). On the suitability of the Thellier method of palaeointensity determinations on pseudo-single-domain and multidomain grains. *Geophysical Journal International*, 146(1), 20–30. <https://doi.org/10.1046/j.0956-540x.2001.01421.x>
- Shcherbakova, V. V., Bakhmutov, V. G., Thallner, D., Shcherbakov, V. P., Zhidkov, G. V., & Biggin, A. J. (2020). Ultra-low palaeointensities from East European Craton, Ukraine support a globally anomalous palaeomagnetic field in the Ediacaran. *Geophysical Journal International*, 220(3), 1928–1946. <https://doi.org/10.1093/gji/ggz566>
- Smirnov, A. V., & Tarduno, J. A. (2005). Thermochemical remanent magnetization in Precambrian rocks: Are we sure the geomagnetic field was weak? *Journal of Geophysical Research*, 110(B6), B06103. <https://doi.org/10.1029/2004JB003445>
- Tauxe, L. (1998). *Paleomagnetic principles and practice*. Kluwer Academic Publishers.
- Tauxe, L., Bertram, H. N., & Seberino, C. (2002). Physical interpretation of hysteresis loops: Micromagnetic modeling of fine particle magnetite. *Geochemistry, Geophysics, Geosystems*, 3(10), 1055. <https://doi.org/10.1029/2001gc000241>
- Thallner, D., Shcherbakova, V. V., Bakhmutov, V. G., Shcherbakov, V. P., Zhidkov, G. V., Poliachenko, I. B., & Biggin, A. J. (2022). New palaeodirections and palaeointensity data from extensive profiles through the Ediacaran section of the Volyn Basalt Province (NW Ukraine). *Geophysical Journal International*, 231(1), 474–492. <https://doi.org/10.1093/gji/ggac186>
- Thellier, E., & Thellier, O. (1959). Sur l'intensité du champ magnétique terrestre dans le passé historique et géologique. *Annales de Geophysique*, 15(3), 285–376.
- Wang, D., & Van der Voo, R. (2004). The hysteresis properties of multidomain magnetite and titanomagnetite/titanomaghemite in mid-ocean ridge basalts. *Earth and Planetary Science Letters*, 220(1–2), 175–184. [https://doi.org/10.1016/s0012-821x\(04\)00052-4](https://doi.org/10.1016/s0012-821x(04)00052-4)
- Xu, S., & Dunlop, D. J. (2004). Thellier paleointensity theory and experiments for multidomain grains. *Journal of Geophysical Research*, 109(B7), B07103. <https://doi.org/10.1029/2004jb003024>
- Zijderveld, J. D. A. (1967). A.C. Demagnetization of rocks: Analysis of results. In D. Collinson, K. M. Creer, & S. K. Runcorn (Eds.), *Methods in paleomagnetism* (pp. 254–286). Elsevier.